Robust Estimation Strategies for a Nonlinear Satellite System

Alex McCafferty-Leroux, Brett Sicard, S. A. Gadsden, and Mohammad Al-Shabi

Abstract Commonly applied in satellites and other complex systems, the Kalman filter (KF) is an optimal estimation strategy and many nonlinear variants have been introduced in practice. A trade-off commonly exists between optimality and robustness. In the presence of unmodeled disturbances, modeling errors, or sub-system failure, non-robust strategies can fail to correctly estimate states, resulting in failure across the system. In the context of Earth observing satellites, this can materialize as internal or environmental disturbances, operational faults, or changes to the system properties, resulting in communication or data loss with performance decline. In this paper, estimation strategies for a nonlinear satellite system are derived and evaluated. Introducing disturbances, modeling errors, and sub-system faults to the simulated dynamics, the state estimation error for each filter is calculated and compared to each other, quantifying robustness. The extended KF and extended sliding in- novation filter (ESIF) are applied, as well as two nonlinear extensions of the second-order SIF and alpha SIF, not previously applied in literature. Computational simulations are performed on an ideal satellite system undergoing an attitude regulation maneuver subjected to selected com- plications. From the results of the experiment, it was concluded that the robust strategies out-performed the conventional EKF when faults were injected, having less error between the estimated and true states.

Keywords Estimation theory · Attitude control · Robust estimation · Sliding innovation filter · Satellite · Fault identification · Kalman Filter

A. McCafferty-Leroux · B. Sicard · S. A. Gadsden (✉)
McMaster University, Hamilton, Canada
e-mail: gadsden@mcmaster.ca

A. McCafferty-Leroux
e-mail: mccaffea@mcmaster.ca

B. Sicard
e-mail: sicardb@mcmaster.ca

M. Al-Shabi
University of Sharjah, Sharjah, United Arab Emirates

P. G. Bradford et al. (eds.), *Proceedings of IEMTRONICS 2024*, Lecture Notes in Electrical Engineering 1228, https://doi.org/10.1007/978-981-97-4784-9_40

1 Introduction

For spacecraft applications, the reliability of the control system is paramount. Satellites and spacecraft must be able to determine the position of themselves and their target, and orient and track those targets with precision. In orbit, satellite systems must be exceptionally accurate to maintain essential Earth operations, such as radio broadcasting and communication, climate monitoring, defense applications, and GPS tracking. Modern satellites are able to achieve short term sub micro-radian accuracy and rotational stability within 10^{-4} deg/s [1, 2], obtaining more accurate and therefore more useful data. Their performance in this regard is dictated by a variety of design factors on both hardware and software levels. Such factors include control, computational efficiency, and specifically, the onboard filtering and state estimation algorithm of the system.

The fundamental objective of estimation is to determine the true state values from measurements. In satellites, states that are typically desirable to have knowledge of are attitude (i.e., quaternion), spacecraft motion, and actuator states. Using system and noise models, a variety of techniques can be applied to extract these true states from noise corrupted measurement signals. Forwarding this information to the control system, a system can achieve more precise control authority over its states with better estimation methods.

Developed by R. Kalman in the 1960s, the Kalman Filter (KF) [3] is the most popular and extensively researched of estimation strategies. The KF is a minimum mean-square error (MMSE) estimator, providing the optimal solution to the linear estimation problem with stochasticity. A recursive process, the KF algorithm predicts the states and error covariance initially based on the system model (i.e., A and B matrices) and the system noise model. Those predictions are then updated/corrected with the Kalman gain matrix, based on measurements and the sensor noise model [3]. For nonlinear systems, the KF equations can be modified such that the time varying system and measurement matrices are incorporated, providing near optimality (though there is no truly optimal nonlinear estimation method). The Extended KF (EKF) is one of the most commonly used nonlinear estimation methods, though more accurate strategies exist, such as the Unscented KF (UKF), the Cubature KF (CKF), and particle filter (PF) [4–6].

Though the EKF provides an near-optimal solution to the estimation problem for a nonlinear dynamic system, it lacks robustness. In the presence of unmodeled disturbances, incorrectly modeled dynamics or noise, or system failure, the KF and EKF methods fail to provide sufficient knowledge of the system. As such, robust estimation methods have been explored in literature to counteract this common issue. Though many methods exist, the following method being explored is the Sliding Innovation Filter (SIF) [7], a relatively new approach to sub- optimal, robust estimation.

In the following paper, robust estimation strategies are examined for a nonlinear satellite system subjected to a variety of faults. The standard EKF is applied and compared to alternative formulations of the robust SIF. The Extended SIF (ESIF), Extended Second-Order SIF (ESIF2), and Extended Alpha SIF (EASIF) are used in experiments, where the latter two are novel formulations for the satellite application. In Sect. 2, a brief literature survey is conducted on robust estimation methods and previous applications of the SIF. Section 3 derives the rigid satellite model being applied, where Sect. 4 derives the estimation strategies being implemented. With Sect. 5, the experiment is conducted and performance is compared by metric of root mean-square error. (RMSE) and ability to estimate the fault. Section 6 offers concluding thoughts and prospects for future work.

2 Literature Review

Addressing the problem of accurate estimation in the presence of uncertainties, robust estimation is introduced. Where optimal estimators fail, robust estimation strategies are sub-optimal, guaranteeing a certain degree of performance for uncertainties under a given bound [8]. Methods such as the robust KF [8] and H_∞ filtering [9] were relatively early adopters of this notion. Hybrid methods were subsequently applied for increased accuracy, integrating the PF and UKF [10, 11]. In 2007, Habibi [12] proposed the Smooth Variable Structure Filter (SVSF) based on variable structure systems. Similar to sliding mode observers [13], the SVSF uses discontinuity hyperplanes, and then the gain of the predictor–corrector estimator is based on a switching term and errors in measurements [7, 12].

Since being established, the SVSF has been improved upon, including a covariance derivation [14], the addressing of chattering effects [15], and the formulation of two-pass and square root variations [16]. Additionally, Gadsden and Al-Shabi derived the SIF, a robust estimation method based on the SVSF [7]. The gain structure of their method was simpler than that of the SVSF, featuring the same variable structure methods utilized in the previous filter, with higher accuracy. Alternative formulations of the SIF have been since introduced based on Interacting Multiple Models (IMM) [17], hybridization with PF and KF [18, 19], and adaptivity in the boundary width definition [20]. Different gain formulations have also been introduced in [21, 22]. The variations of the SIF have been applied to a variety of dynamic systems, up until this work, none of which have been a satellite. Additionally, the methods outlined in [21, 22] have not been extended to nonlinear dynamics.

3 Satellite Model

The satellite under study is modeled as a rigid spacecraft without consideration for passive control methods or environmental disturbances. For control and estimation, the kinematic equations of the attitude quaternion and the dynamic relationship between the reaction wheel momentum contribution and the body spin rate of the satellite are utilized. They are expressed as a time-varying state space model.

3.1 Kinematic Equations

The kinematic equations of the satellite provide a relationship of how the attitude quaternion $\mathbf{q}$ changes based on the body angular velocities about the Cartesian axes ω, and the current quaternion vector. The quaternion is essential in attitude determination since it expresses the attitude matrix as a homogeneous quadratic function of its elements [23], implying that the attitude can be evaluated without transcendental trigonometric functions or singularities [23]. The definition of a quaternion is provided in [23], where in this work the identity quaternion is defined as $\mathbf{q}_I = [0\ 0\ 0\ 1]^T$. The attitude kinematic equation is presented below as Eq. 1, which is derived in [23].

$$\mathrm{q}_{\dot{\mathrm{B}}\mathrm{I}}(t) = \frac{1}{2}[\omega_B^{\mathrm{BI}}\otimes]\mathrm{q}_{\mathrm{BI}}(t) \tag{1}$$

where the values are in terms of the body frame B with respect to the inertial frame I. The skew symmetric matrix term of the satellite body angular velocities is used to preserve the quaternion norm after derivation [23]. The definition is presented below as Eqs. 2 and 3. The ω term is the body angular velocity vector about the three principal axes.

$$\left[\omega_B^{\mathrm{BI}}\otimes\right] = \begin{bmatrix} -[\omega\times] & \omega(t) \\ -\omega(t)^T & 0 \end{bmatrix} \tag{2}$$

$$[\omega\times] = \begin{bmatrix} 0 & -\omega_z(t) & \omega_y(t) \\ \omega_z(t) & 0 & -\omega_x(t) \\ -\omega_y(t) & \omega_x(t) & 0 \end{bmatrix} \tag{3}$$

3.2 Dynamic Equations

The dynamic model of the satellite considers the angular momentum, inertia, and how external and internal forces impact the attitude of the satellite. For the type of attitude control under analysis, the satellite can only rotate in three axes about itself, and lateral movements/perturbations are not considered.

We can define the angular momentum of the satellite with respect to the body frame, $\mathbf{H}$, as the product of the moment of inertia (MOI) matrix of the satellite with respect to the body center of mass, J^c, and the body rotational velocity vector, ω^{BI}, which is the net torque acting on the system [23]. It can be rearranged to the more convenient form of Eq. 4.

$$\omega_B^{\mathrm{BI}}(t) = \left(J_B^c\right)^{-1}\mathbf{H}_B^c(t) \tag{4}$$

The rigid body dynamics of the satellite with respect to the body frame (de- noted by B) are more simply calculated than that of the inertial frame (denoted by I), since the MOI matrix becomes time variant in the latter case. Applying time derivative rules for vectors and the fact that $\dot{\mathbf{H}}_I^c = \mathbf{L}_I^c$, Eq. 5 can be used to describe the rate of angular momentum of the satellite with respect to the body frame [23].

$$\dot{\mathbf{H}}_B^c(t) = \mathbf{L}_B^c(t) - \omega_B^{\mathrm{BI}}(t) \times \mathbf{H}_B^c(t) \tag{5}$$

Note that in Eq. 5 the term, $\mathbf{L}$ acting on the body represents external torques. Using Eq. 4, we can define the overall angular momentum about the satellite CoM as the combination of the angular momentum of the body and the angular momentum contributed by the reaction wheel actuators [23], as Eq. 6.

$$\mathbf{H}_B(t) = \mathbf{H}_B^{\mathrm{B}}(t) + \mathbf{H}_B^{\mathrm{W}}(t) = J_B\omega_B^{\mathrm{BI}}(t) + \mathbf{H}_B^{\mathrm{W}}(t) \tag{6}$$

The angular momentum of the four reaction wheels (terms denoted by W) is then defined as Eq. 7, as a function of each individual wheel's inertia and angular velocity, J and ω respectively [23]. Applying a redundant configuration, the spin axis of each wheel is mapped with respect to the body frame through the dimensionless matrix, W_N.

$$\mathbf{H}_B^{\mathrm{W}}(t) = W_N\mathbf{H}_W^{\mathrm{W}}(t) = W_N J_W^{\mathrm{W}}\omega_W^{\mathrm{W}}(t) \tag{7}$$

We can observe in Eq. 8 that the time rate of change of the term $\mathbf{H}^{\mathrm{W}}$ is the torque vector in the three principal directions imposed on the satellite body, generated by the reaction wheels. Since we have direct authority over the momentum magnitude for each wheel, this is also referred to as the control input, typically defined as $\mathbf{u}$.

$$\dot{\mathbf{H}}_B^{\mathrm{W}}(t) = \mathbf{L}_B^{\mathrm{W}}(t) = \mathbf{u}(t) \tag{8}$$

Deriving the dynamic relation in terms of the time rate of change of the angular velocity of the satellite body. Using Eq. 4, we can substitute in Eq. 6 to produce Eq. 9, the total angular momentum of the satellite.

$$\mathbf{H}_B(t) = J_B\omega_B^{\mathrm{BI}}(t) + W_N J_W^{\mathrm{W}}\omega_W^{\mathrm{W}}(t) \tag{9}$$

Differentiating and isolating for the derivative of the body angular velocity vector, we produce the final dynamic model for the satellite [23] as Eq. 10.

$$\dot{\omega}_B^{\mathrm{BI}} = \left(J_B^c\right)^{-1}\left[\mathbf{L}_B^c - \mathbf{u} - \omega_B^{\mathrm{BI}} \times \left(J_B^c\omega_B^{\mathrm{BI}} + W_N J_W^{\mathrm{W}}\omega_W^{\mathrm{W}}\right)\right] \tag{10}$$

For a representation of how the designed control torque relates to the reaction wheel dynamics, we can apply Eq. 8 [24] and the mapping between wheel and body axes. Equation 11 is incorporated into the state space.

$$\dot{\omega}^{W}(t) = J_{W}^{-1}\mathbf{T}^{W}(t) = J_{W}^{-1}W_{N}\mathbf{u}(t) \tag{11}$$

4 Filter Derivation

4.1 Extended Kalman Filter

The recursive discrete EKF algorithm is separated into the prediction and update stages. The prediction stage (a priori) estimates the state vector $\mathbf{x}\hat{}_{k+1|k}$ and the state error covariance, $P_{k+1|k}$, using Eqs. 12 and 13 below [3].

$$\hat{\mathbf{x}}_{k+1|k} = f\left(\hat{\mathbf{x}}_{k|k}, \mathbf{u}_{k}\right) \tag{12}$$

$$P_{k+1|k} = A_{k}P_{k|k}A_{k}^{T} + Q_{k} \tag{13}$$

The nonlinear model for the system (Eq. 12) can also be expressed in terms of the system and control matrices, A_k and B_k, where A_k is applied in Eq. 13. For improved accuracy, the nonlinear Eq. 12 is used for the a priori state estimate. The system noise covariance is denoted as Q_k. The up- date stage (a posteriori) determines the corrected covariance $P_{k+1|k+1}$ and state $\mathbf{x}\hat{}_{k+1|k+1}$ values through the computation of the Kalman gain, K_{k+1}. Applying this gain produces the optimal estimate (in linear systems) and the process is illustrated by the following equations [3]. The parameters R_{k+1} and S_{k+1} are the measurement noise covariance and the innovation covariance, respectively.

$$S_{k+1} = C_{k+1}P_{k+1|k}C_{k+1}^{T} + R_{k+1} \tag{14}$$

$$K_{k+1} = P_{k+1|k}C_{k+1}^{T}S_{k+1}^{-1} \tag{15}$$

$$\hat{\mathbf{x}}_{k+1|k+1} = \hat{\mathbf{x}}_{k+1|k} + K_{k+1}\left(z_{k+1} - h\left(\hat{\mathbf{x}}_{k+1|k}\right)\right) \tag{16}$$

$$P_{k+1|k+1} = (I - K_{k+1}C_{k+1})P_{k+1|k}(I - K_{k+1}C_{k+1})^{T} + K_{k+1}R_{k+1}K_{k+1}^{T} \tag{17}$$

4.2 Sliding Innovation Filter

Originally proposed by Gadsden and Al-Shabi [7], the SIF is a predictor–corrector estimation strategy like the KF and utilizes most of the same equations (Eqs. 12, 13, 14, 16, 17). The Extended SIF (ESIF) was derived in the same publication, for the nonlinear system case.

For the gain, it is instead calculated as a function of the innovation $\tilde{\mathbf{z}}_{k+1|k}$ (i.e., the difference between the measurement and estimated measurement, $C_{k+1}\,\hat{\mathbf{x}}_{k+1|k}$), the measurement matrix C, and the width of the sliding boundary layer δ. The sub-optimality is a consequence of omitting the state error covariance in this calculation [7].

Illustrated in Fig. 1 above, the estimated state is driven towards an existence subspace (defined by the boundary layer width, δ) and bounded close to the true trajectory [7]. The estimate is maintained within the boundary due to the switching characteristic of the gain, defined in Eq. 18. Note also that the prediction stage must be augmented with Eq. 19 to calculate the innovation.

$$K_{k+1} = C^{+}\mathrm{sat}\left(\frac{\left|\widetilde{\mathbf{z}}_{k+1|k}\right|}{\delta}\right) \tag{18}$$

$$\widetilde{\mathbf{z}}_{k+1|k} = \mathbf{z}_{k+1} - C_{k+1}\widehat{\mathbf{x}}_{k+1|k} \tag{19}$$

The stability of this gain is proven, provided the boundary layer is equal to or greater than a specified magnitude, defined in [7]. The size of δ can be determined with this equation or tuned. A width larger than the maximum value of uncertainties will provide smooth estimates, where widths smaller than this value results in chattering [7].

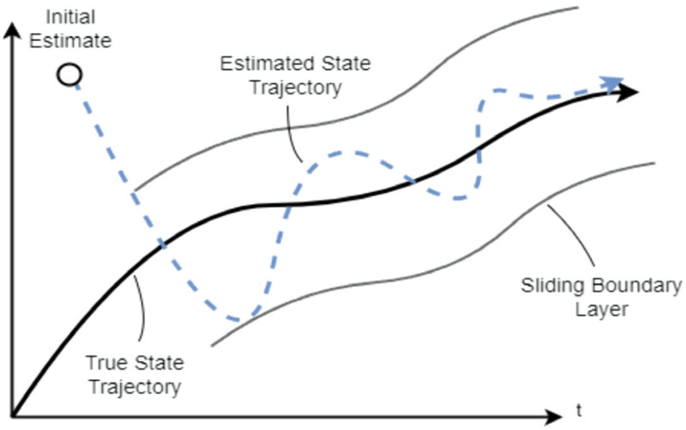

Fig. 1 SIF behaviour illustration (adapted from [7])

4.3 Extended Second-Order SIF

Following the successful application of the SIF, alternative formulations and hybrid methods have been derived [18, 19, 25]. A variation that features an alternate gain formulation is the Second-Order SIF (SIF2) [21]. Deriving the gain with an alternative Lyapunov function found in [26], the method was proposed to increase the accuracy of the robust sub-optimal estimator, using innovation terms from two separate time steps. This notion was verified in the simulation of a linear electrohydrostatic actuator (EHA) model. The gain for the SIF2 is calculated based on Eq. 20, and the update stage is augmented with 19.

$$K_{k+1} = C^{+}\text{sat}\left(\left|\frac{\widetilde{\mathbf{z}}_{k+1|k}}{\delta} - \frac{\widetilde{\mathbf{z}}_{k|k}}{2\delta}\right|\right) \tag{20}$$

The stability of this gain is proven in [21]. In the following section, the SIF2 is proposed to be extended to nonlinear systems, where the gain expressed in Eq. 20 is utilized in the aforementioned EKF equations for the satellite system.

4.4 Extended Alpha-SIF

In addition to the SIF2, the alpha SIF (ASIF) was derived to improve the performance of the SIF with a simple adjustment mechanism based on a forgetting factor, α [22]. The forgetting factor optimizes measurement confidence, reducing the lack of confidence as a result of noise. The simplified mechanism is beneficial for high order systems, as boundary layer width definition is necessary for each state [22]. In the simulations from Al-Shabi and Gadsden, the ASIF was demonstrated to perform better than the KF in the presence of uncertainties, where the superiority to the SIF was slight.

$$K_{k+1} = \alpha C^{+} \tag{21}$$

The gain determination is represented by Eq. 21 for the ASIF, again extended to a nonlinear satellite system in the subsequent section for the novel application. The constraint applied to the forgetting factor α is that it must be between 0 and 2 (including). The characteristics of forgetting factor values was determined in [22].

5 Experimental Results

5.1 System Parameters

In this section, the EKF, ESIF, ESIF2, and EASIF are applied to a nonlinear satellite attitude control experiment with faults and noise. The system is based on the geometry of a lab nanosatellite simulator, and is linearized to a time-varying state space form and discretized, with an eleven-entry state vector and constant MOI and control matrix B. The full nonlinear system is presented below as Eqs. 22 and 23, abusing notation for brevity. Note as well that the system measurements are assumed to correspond exactly with the states, where the measurement matrix C is identity.

$$\dot{\mathbf{x}}_k = \begin{bmatrix} \frac{1}{2}\left[\omega_k^B \otimes\right]\mathbf{q}_k \\ J_B^{-1}\left[\omega_k^B \times \left(J_B\omega_k^B + W_N J_W \omega_k^W\right)\right] \\ 0_{4\times 11} \end{bmatrix} + \begin{bmatrix} 0_{4\times 3} \\ -J_B^{-1} \\ J_W^{-1} W_N^{+} \end{bmatrix} \mathbf{u}_k + \mathbf{w}_k \tag{22}$$

$$\mathbf{z}_k = C\mathbf{x}_k + \mathbf{v}_k \tag{23}$$

The system is simulated in Matlab using a sampling rate T of 10 ms. The $\mathbf{w}$ and $\mathbf{v}$ terms are the process and sensor noise of the system. For the ideal case, the reaction wheel and system inertia, and geometric reaction wheel mapping are known, with noise modeled as zero-mean Gaussian, with known noise co- variances, Q and R. The ideal known parameters are defined below as Eq. 24.

$$J_B = \begin{bmatrix} 0.0196 & -0.0033 & -0.0010 \\ -0.0033 & 0.0217 & 0.0009 \\ -0.0010 & 0.0009 & 0.0287 \end{bmatrix} \mathrm{kgm}^2$$

$$J_W = 1.740138 \times 10^{-5}\mathrm{kgm}^2 \tag{24}$$

$$W_N = \begin{bmatrix} 0.5 & 0.5 & -0.5 & -0.5 \\ -0.5 & 0.5 & -0.5 & 0.5 \\ -1/\sqrt{2} & -1/\sqrt{2} & -1/\sqrt{2} & -1/\sqrt{2} \end{bmatrix}$$

$$Q = 1 \times 10^{-9} I \quad R = 10Q$$

The reaction wheel inertias are assumed identical. The reaction wheel mapping W_N was derived considering the four wheel pyramidal configuration utilized. The maximum velocity of the reaction wheels is 10 000 rpm and the system is subjected to this constraint. The initial condition of the state error covariance P was defined as $10Q$, and there is no error between the first estimate and the initial state. The entries of the state vector $\mathbf{x}$ correspond to the quaternion, body angular rates, and reaction wheel speed, respectively.

$$\mathbf{x}_0 = \left[\, \mathbf{q}_0 \; \omega_0^B \; \omega_0^W \,\right]^T \tag{25}$$

For the control scheme, a simple PD controller was designed to achieve the desired state with minimal overshoot, reasonable rise time, and no steady state error, as a function of body angular velocity error ω_e and quaternion error δq. The gains were tuned as $K_p = 0.025$ and $K_d = 0.05$, where the control law is presented as Eq. 26.

$$\mathbf{u}_k = K_p \delta \mathbf{q}_{e,k}^{1:3} + K_d \omega_{e,k} \tag{26}$$

where the first three entries of the error quaternion are utilized, calculated based on the current and desired quaternion, with normalization (essential in quaternion computation). Further details can be found in [23].

5.2 Experiment Methodology and Results

The experiment is a 5000 data point simulation of a simple state regulation attitude control maneuver, with integrated estimation. A desired attitude described by quaternion and angular velocity is given to the system, made achievable from some initial condition provided the control law in Eq. 26.

The attitude control simulation without system faults is presented in Figure 2. For the four estimation strategies tested, the system was evaluated for the ideal case, as well as for four different types of faults:

Unmodeled Disturbance A constant sinusoidal perturbation is applied to the system to simulate some unmodeled disturbance that the estimator has no knowledge of. This could represent some combination of gravity gradient, magnetic, or aerodynamic torque, common in spacecraft. The arbitrary disturbance vector is presented as Eq. 27 below.

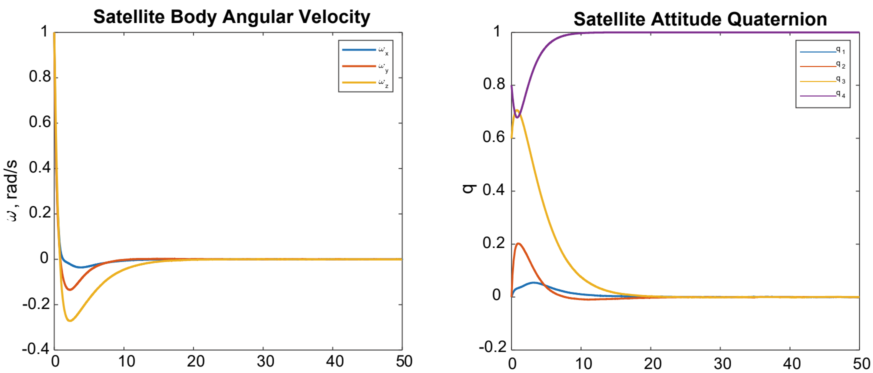

Fig. 2 Attitude control maneuver

$$L_B = \left[\, 0.001\sin(2\pi t/5)\ 0.001\sin(2\pi t/5)\ 0.001\sin(2\pi t/5) \,\right]^T \tag{27}$$

System Modeling Error In the system model utilized by the estimator, a large discrepancy is introduced between the modeled and real inertias. To inhibit performance, the model body inertia was defined as being 5 times greater than the true MOI. Modeling errors such as these can manifest themselves from mischaracterizing the system elements or materials.

System Fault For this type of fault, the alternate inertia is instead applied to the plant partway through the simulation, resulting in unexpected (but stable) control performance. The body inertia, J_B is increased by 0.1 kgm^2 on the J_{xx} element, simulating some sudden imbalance on the system, which can represent payload deployment or spacecraft damage.

Reaction Wheel Friction A simple viscous and Coulomb friction model is applied as a disturbance to the system, $\mathbf{f}_k$ as a function of the reaction wheel velocity. Parameters c and b were obtained as 0.8795 10^{-3} and 5.16 10^{-6} Nms/rad, respectively, from [24]. The disturbance is unmodeled in the estimation stage, and constant through the simulation. The torque on the system as a result of this friction is modeled below as Eq. 28, where the reaction wheel mapping is applied to express its impact in the body frame. Equation 29 shows how the torque generates the disturbance f_k, which is added onto the system dynamics in the same manner as process noise $\mathbf{w}_k$.

$$\mathbf{u}_k^f = -bW_N\omega_k^W - cW_N\operatorname{sign}\left(\omega_k^W\right) \tag{28}$$

$$f_k = \begin{bmatrix} 0_{4\times 3} \\ -J_B^{-1} \\ J_W^{-1}W_N^+ \end{bmatrix}\left(-bW_N\omega_k^W - cW_N\operatorname{sign}\left(\omega_k^W\right)\right) \tag{29}$$

The RMSE tables for each fault situation are presented in the following section. Though the state and associated RMSE are an 11 entry vector, for the purposes of presentation, only the RMSE of the angular velocity will be tabulated, as they consisted of the largest inaccuracies and affect the quaternion directly. For each fault case, the estimation error between the strategies in the x axis (typically most affected) are presented, highlighting the main result, as well as a snapshot of the estimated and true angular velocity waveforms for that axis.

For the ESIF and ESIF2, the boundaries were tuned to yield the smallest error. For the EASIF, the parameter α was chosen according to [22]. It is known for the simulation that the measurement noise covariance R is larger than that of the process noise Q, therefore α should be less than one. This parameter varies across simulations. Tunable filter parameters for each simulation case are presented in Table 1, where the δ values are constant for each state. Since the noise levels are relatively low, the simulation results were not averaged across a batch and are fairly repeatable.

Table 1 Simulation case parameters

Parameter	Ideal	Case 1	Case 2	Case 3	Case 4
δ_{ESIF}	5×10^{-4}	5×10^{-5}	5×10^{-4}	5×10^{-4}	5×10^{-4}
δ_{ESIF_2}	5×10^{-4}	5×10^{-5}	5×10^{-4}	5×10^{-4}	5×10^{-4}
α	0.5	0.9	0.95	0.95	0.99

For the ideal case, the results are presented in Table 2. As expected, with assumed knowledge of the system and process noise covariance, the EKF out- performs the sub-optimal SIFs.

In the presence of some unmodeled external disturbance, the superiority of the EKF is surpassed by the robust methods, evident in Table 3. In the error profile between the true and estimated states, the EKF could not achieve convergence for the angular velocity, where the error oscillated at a similar waveform to the disturbance. The performance of tuned SIF variations was highly accurate, though the difference between variations was minimal. High frequency gain switching was evident as a consequence of its accuracy, a factor of 10 over the EKF (Fig. 3).

For the case of the system model being subjected to modeling errors in the estimator, the SIF variations demonstrated to have significantly less maximum and root mean-square error. Table 4 below summarizes the performance. It should be noted however that the largest EKF errors were at the start of the simulation and converged quickly and well (see Fig. 4), accounting for the inertia discrepancy through the Kalman gain. After convergence, the average maximum error amplitudes were approximately 2×10^{-4}, on par with the SIF error waveforms. The EASIF featured the same behavior as the EKF, and as such the estimates were not as accurate as the ESIF and ESIF2, each having negligible difference.

Table 2 Ideal case estimation performance (no faults)

RMSE ($\times 10^{-4}$)	EKF	ESIF	ESIF2	EASIF
ω_x	0.49565	0.58098	0.60751	0.60950
ω_y	0.52179	0.60246	0.59073	0.59673
ω_z	0.52541	0.60497	0.60550	0.60281
Σ_{RMSE}	1.54285	1.78842	1.80374	1.80903

Table 3 Unmodeled external disturbance estimation performance

RMSE ($\times 10^{-3}$)	EKF	ESIF	ESIF2	EASIF
ω_x	1.22626	0.10026	0.10127	0.10325
ω_y	1.02012	0.10036	0.10027	0.9903
ω_z	0.67894	0.09998	0.09893	0.09434
Σ_{RMSE}	2.92531	0.30061	0.30047	0.29663

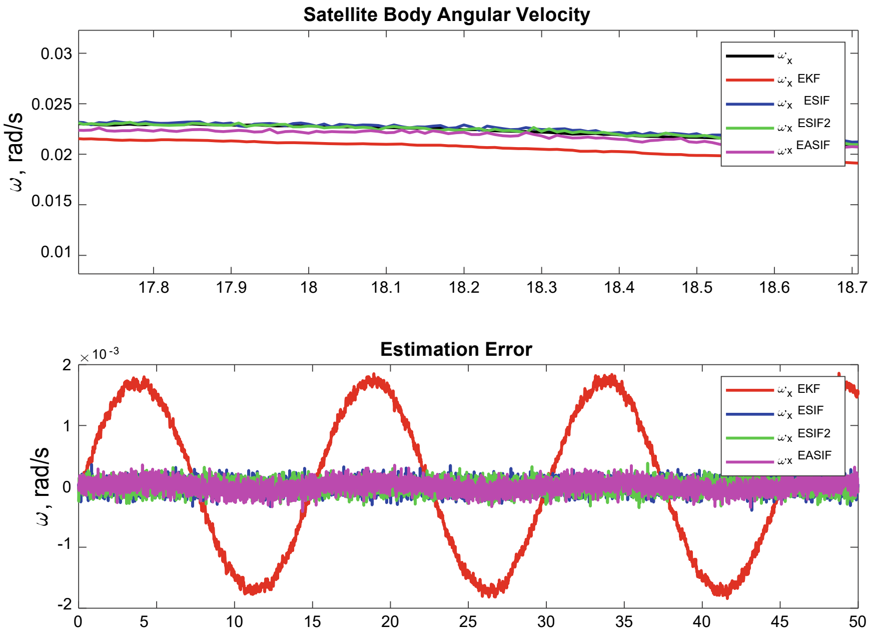

Fig. 3 Estimation performance (external disturbance)

Table 4 Modeling error estimation performance

RMSE ($\times 10^{-3}$)	EKF	ESIF	ESIF2	EASIF
ω_x	3.89879	0.07114	0.07065	0.12599
ω_y	3.16071	0.07495	0.07637	0.11635
ω_z	3.73808	0.08471	0.08426	0.12039
Σ_{RMSE}	10.7976	0.23079	0.23128	0.36273

When the plant is subjected to an unexpected fault causing an alteration to system geometry, the robust estimation methods again were demonstrated to surpass the EKF in terms of performance. The results are presented in Table 5. Note again however, the same phenomena as in the previous test case, where errors were initially large but convergence occurred within the same small bounds as the SIFs (approx. 2 10^{-4} amplitude, see Fig. 5). As expected, the error on the body x axis is the largest. The performance of ESIF and ESIF2 was very similar, slightly better than the EASIF.

Considering reaction wheel friction, robust methods are able to reject the constant disturbance, where if the friction is unmodeled in the EKF, a constant error results, as seen in Fig. 6. The results of this experiment are presented in Table 6. With the control law selected, steady state error results and the difference in performance across the SIF variations was negligible.

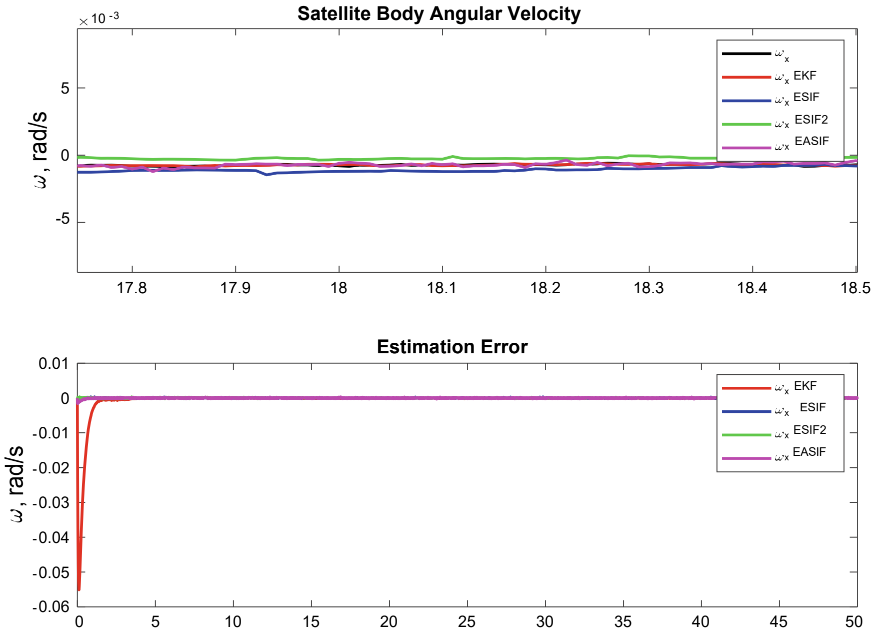

Fig. 4 Estimation performance (modeling error)

Table 5 System fault estimation performance

RMSE ($\times 10^{-3}$)	EKF	ESIF	ESIF2	EASIF
ω_x	2.82871	0.09142	0.08955	0.11311
ω_y	0.60520	0.07740	0.07725	0.09615
ω_z	0.38843	0.07262	0.07218	0.09622
Σ_{RMSE}	3.82234	0.24144	0.23899	0.30548

6 Conclusions

In this paper, three robust estimation strategies were simulated and compared to the standard EKF. For the satellite attitude control experiments, the alternate nonlinear formulations of the SIF demonstrated robustness to a variety of common spacecraft faults, yielding more accurate results than the more optimal estimator. The foundations of these estimation strategies were first formulated by Gadsden and Al-Shabi in [7, 21, 22]. Two of these estimation strategies, the SIF2 and ASIF have not been extended to nonlinear systems in previous literature. A background on optimal and robust estimation was first provided, where the satellite dynamics and filter equations were subsequently outlined.

The four estimation strategies under study were applied to four different fault cases, of unmodeled external and internal disturbance, modeling error, and system

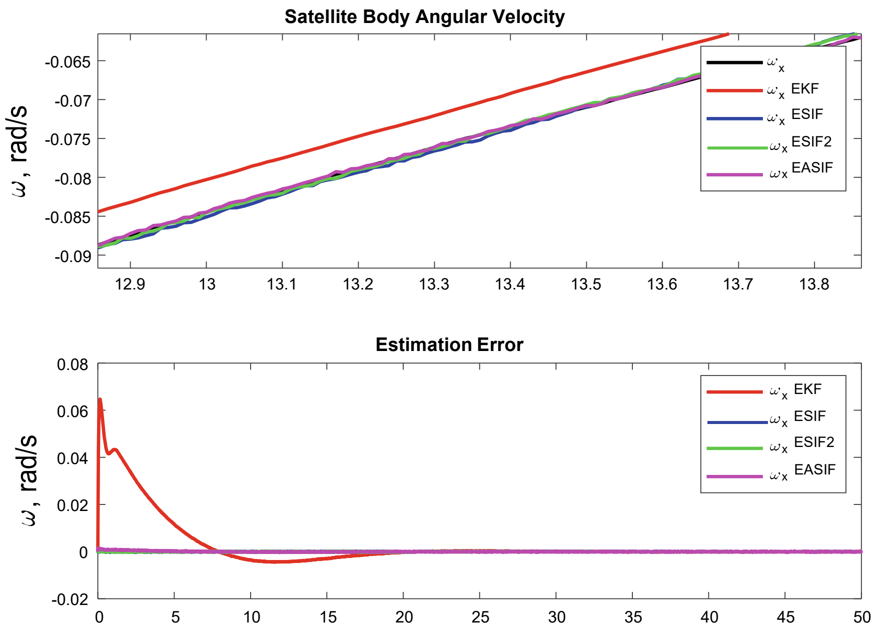

Fig. 5 Estimation performance (system fault)

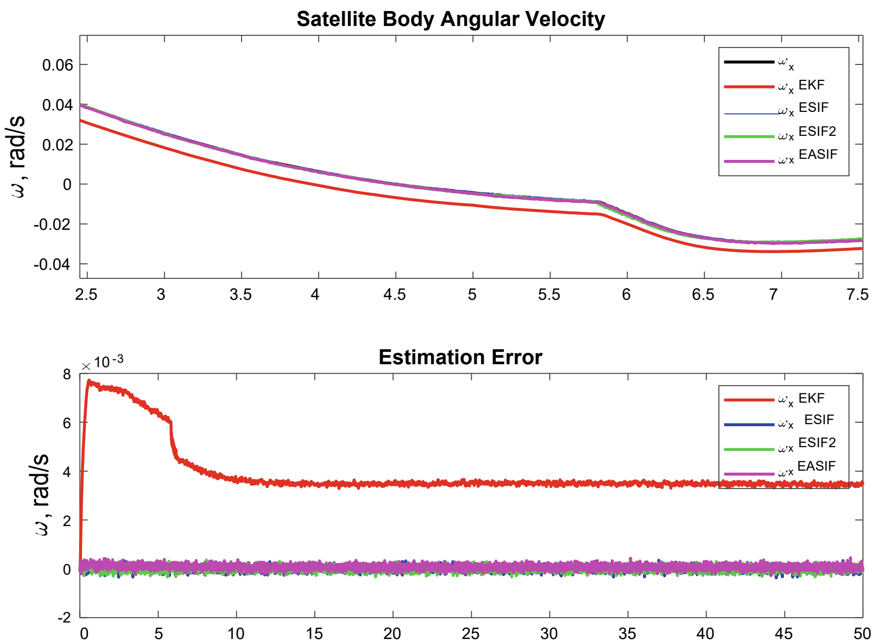

Fig. 6 Estimation performance (internal disturbance)

Table 6 Reaction wheel friction estimation performance

RMSE ($\times 10^{-4}$)	EKF	ESIF	ESIF2	EASIF
ω_x	4.08997	0.10034	0.10121	0.09879
ω_y	3.02464	0.09907	0.10105	0.09973
ω_z	9.11852	0.10071	0.10033	0.10305
Σ_{RMSE}	16.2331	0.30012	0.30259	0.30157

fault. The results demonstrated that the SIF variations are significantly more robust to these faults, specifically the unmodeled disturbances. The modeling and system errors introduced large initial state estimation errors for the EKF and EASIF, but converged to small magnitudes. For the ideal case, the optimal EKF outperformed the SIFs. Across the SIFs in fault cases 2 and 4, the difference in performance was negligible. In those cases, the fine tuning of δ and α might yield improved results. For cases 1 and 3, the EASIF was out- performed by the ESIF and ESIF2. The results demonstrated the applicability of computationally light robust estimation strategies for spacecraft and fault identification.

In terms of future work, the implementation of an adaptive boundary width would add to the performance of the estimator, not having to manually tune the vector δ. The change in this width could also be used to detect faults, as discussed in [20]. These formulations of SIF could also be applied to a real system, either in-loop or to experiment data. Additionally, it is worth noting that the EKF was observed to perform significantly worse than the SIF and variations when a lower sampling rate was simulated. It is suggested that a future avenue of work could involve exploring robust estimation with the SIF for systems that are lacking computational power or under the influence of denial-of-service (DoS) cyberattacks, or other threats that artificially decrease the computation ability of the system.

References

1. Li L, Yuan L, Wang L, Zheng R, Wu Y, Wang X (2021) Recent advances in precision measurement and pointing control of spacecraft. Chin J Aeronaut 34(10):191–209
2. Yoshida N, Takahara O, Kodeki K (2013) Spacecraft with very high pointing sta bility: experiences and lessons learned. In: IFAC proceedings volumes, vol 46, no 19, pp 547–552, 2013, 19th IFAC symposium on automatic control in aerospace
3. Kalman RE (1960) A new approach to linear filtering and prediction problems. Trans ASME–J Basic Engin 82, Series D, pp 35–45
4. Julier SJ, Uhlmann JK (1997) New extension of the kalman filter to nonlinear systems. In: Signal processing, sensor fusion, and target recognition VI, vol 3068. Spie, pp 182–193
5. Arasaratnam I, Haykin S (2009) Cubature kalman filters. IEEE Trans Autom Control 54(6):1254–1269
6. Djuric P, Kotecha J, Zhang J, Huang Y, Ghirmai T, Bugallo M, Miguez J (2003) Particle filtering. IEEE Signal Process Mag 20(5):19–38
7. Gadsden SA, Al-Shabi M (2020) The sliding innovation filter. IEEE Access 8:96 129–96 138

8. Xie L, Soh YC (1994) Robust kalman filtering for uncertain systems. Syst Control Lett 22(2):123–129
9. Berman N, Shaked U (2005) H-infinity filtering for nonlinear stochastic systems. In: Proceedings of the 2005 IEEE international symposium on, mediterrean conference on control and automation intelligent control, 2005, pp 749–754
10. Li W, Jia Y (2010) H-infinity filtering for a class of nonlinear discrete-time systems based on unscented transform. Signal Process 90(12):3301–3307
11. Wang Q, Li J, Zhang M, Yang C (2011) H-infinity filter based particle filter for maneuvering target tracking. Progr Electromagn Res B 30:103–116
12. Habibi S (2007) The smooth variable structure filter. Proc IEEE 95(5):1026–1059
13. Yan X-G, Edwards C (2007) Nonlinear robust fault reconstruction and estimation using a sliding mode observer. Automatica 43(9):1605–1614
14. Gadsden S, Habibi SR (2010) A new form of the smooth variable structure filter with a covariance derivation. In: 49th IEEE conference on decision and control (CDC), pp 7389–7394
15. Al-Shabi M, Gadsden S, Habibi S (2013) Kalman filtering strategies utilizing the chattering effects of the smooth variable structure filter. Signal Process 93(2):420–431
16. Gadsden SA, Lee AS (2017) Advances of the smooth variable structure filter: square-root and two-pass formulations. J Appl Remote Sens 11(1):015018
17. Lee AS, Wu Y, Gadsden SA, AlShabi M (2024) Interacting multiple model estimators for fault detection in a magnetorheological damper. Sensors 24(1)
18. Hilal W, Alsadi N, Gadsden SA, AlShabi M (2023) An adaptive SIF and KF estimation strategy for fault detection based on the NIS metric. In: Chen G, Pham KD (eds) Sensors and systems for space applications XVI, vol 12546, International Society for Optics and Photonics. SPIE, p 125460S
19. Alsadi N, Hilal W, Gadsden SA, Al-Shabi M (2023) Derivation of the sliding innovation information filter for target tracking. In: Kadar I, Blasch EP, Grewe LL (eds) Signal processing, sensor/information fusion, and target recognition XXXII, vol 12547, International Society for Optics and Photonics. SPIE, p 1254708
20. Lee AS, Gadsden SA, Al-Shabi M (2021) An adaptive formulation of the sliding innovation filter. IEEE Signal Process Lett 28:1295–1299
21. Gadsden SA, AlShabi MA, Wilkerson SA (2021) Development of a second- order sliding innovation filter for an aerospace system. In: Chen G, Pham KD (eds) Sensors and systems for space applications XIV, vol 11755, International Society for Optics and Photonics. SPIE, p 117550T
22. AlShabi M, Gadsden SA (2022) Formulation of the alpha sliding innovation filter: a robust linear estimation strategy. Sensors 22(22)
23. Markley FL, Crassidis JL (2014) Fundamentals of spacecraft attitude determina tion and control, vol 1286. Springer
24. Castaldi P, Nozari HA, Sadati-Rostami J, Banadaki HD, Simani S (2022) Intelligent hybrid robust fault detection and isolation of reaction wheels in satellite attitude control system. In: 2022 IEEE 9th international workshop on metrology for aerospace (MetroAeroSpace), 2022, pp 441–446
25. Lee AS, Hilal W, Andrew Gadsden S, Al-Shabi M (2003) Combined kalman and sliding innovation filtering: An adaptive estimation strategy. Measurement 218:113228
26. Afshari HH, Gadsden SA, Habibi S (2019) A nonlinear second-order filtering strategy for state estimation of uncertain systems. Signal Process 155:182–192